

Phase diagram of insulating crystal and quantum Hall states in ABC-stacked trilayer graphene

R. Côté,¹ Maxime Rondeau,¹ Anne-Marie Gagnon,¹ and Yafis Barlas²

¹*Département de physique, Université de Sherbrooke, Sherbrooke, Québec, J1K 2R1, Canada*

²*Department of Physics and Astronomy, University of California, Riverside, CA 92521*

(Dated: August 13, 2012)

In the presence of a perpendicular magnetic field, ABC-stacked trilayer graphene's chiral band structure supports a 12-fold degenerate $N = 0$ Landau level (LL). Along with the valley and spin degrees of freedom, the zeroth LL contains additional quantum numbers associated with the LL orbital index $n = 0, 1, 2$. Remote inter-layer hopping terms and external potential difference Δ_B between the layers lead to LL splitting by introducing a gap Δ_{LL} between the degenerate zero-energy triplet LL orbitals. Assuming that the spin and valley degrees of freedom are frozen, we study the phase diagram of this system resulting from competition of the single particle LL splitting and Coulomb interactions within the Hartree-Fock approximation at integer filling factors. Above a critical value Δ_{LL}^c of the external potential difference i.e, for $|\Delta_{LL}| > \Delta_{LL}^c$, the ground state is a uniform quantum Hall state where the electrons occupy the lowest unoccupied LL orbital index. For $|\Delta_{LL}| < \Delta_{LL}^c$ (which corresponds to large positive or negative values of Δ_B) the uniform QH state is unstable to the formation of a crystal state at *integer* filling factors. This phase transition should be characterized by a Hall plateau transition as a function of Δ_{LL} at a fixed filling factor. We also study the properties of this crystal state and discuss its experimental detection.

PACS numbers: 73.21.-b, 73.22.Gk, 72.80.Vp

I. INTRODUCTION

Quantum Hall studies of graphene's two dimensional electron system provided the earliest confirmation of the massless Dirac character of its bands^{1,2}. Similar studies have also confirmed the massive Dirac character of bilayer graphene bands^{3,4} and are making progress toward revealing the distinct bands of ABA and ABC trilayers⁵. Few layer graphene systems stacked in different ways give rise to distinct electronic properties at relevant energy scales which introduces an entirely new class of two-dimensional electron gas (2DEG) systems. Recent theoretical work has indicated that except for very weak fields, multilayer graphene systems^{6,7} can be classified as a new class of 2DEG systems from here on referred to as chiral 2DEGs (C2DEGs)⁸. C2DEG models provide an accurate description of the low-energy properties of few-layer graphene systems with a variety of different stacking arrangements consistent with symmetries.

Properties of quasiparticle excitations in C2DEGs are determined by their chirality index J . The quasiparticle dispersion is given by $\epsilon_J \sim |p|^J$ (where p is momentum quantum number measured about some special points in the Brillouin zone) and quasiparticles exhibit a Berry phase of $J\pi$. These properties lead to an unusual Landau quantization. Due to this, integer quantum Hall effects (IQHEs) in C2DEGs are remarkably different from that of semiconducting 2DEGs. Examples of this are quantum Hall effects in single layer, bilayer and trilayer graphene which exhibit unusual IQHEs described by Dirac continuum models. At low-energies these systems represent the $J = 1$, $J = 2$ and $J = 3$ instances of the C2DEGs⁶ model respectively. Another unique property of C2DEGs is the presence of a zero-energy LL with degenerate LL

orbitals $n = 0, \dots, J - 1$. Speaking loosely, quantum states corresponding to cyclotron orbits with different radius, which would have different energies in an ordinary two-dimensional electron gas, are degenerate. This degeneracy is, of course, on top of the normal Landau level *one-state-per-flux-quantum* degeneracy and the four-fold degeneracy already present due to spin and valley degrees of freedom. The zero-energy LL is thus $4J$ -fold degenerate.

Naively it can be anticipated that Coulomb interactions will lift the $4J$ -fold degeneracy of the $N = 0$ LL by producing spontaneously broken-symmetry ground states with spin, valley pseudospin and LL orbital pseudospin polarizations. As a consequence, one would expect quantum Hall plateaus at all intermediate integer values of the filling factors from $\nu = -2J + 1$ to $\nu = 2J$ ⁹⁻¹¹. It turns out that this expectation only holds for $J \leq 2$ C2DEGs, whereas for $J > 2$ insulating states in the top-most LL appear generically, which leads to a disappearance of certain Hall plateaus¹² from the above sequence and a quantization of the Hall conductivity σ_{xy} at a value corresponding to the *adjacent* interaction driven integer quantum Hall plateau (for example, $\sigma_{xy} = -6e^2/h$ when $\nu = -5$). Thus, the presence of wave functions with different spatial structures appearing at the same energy has important consequences on the interaction driven QH states in ABC-trilayer graphene (i.e. C2DEG systems with chirality index $J > 2$). In particular due to the LL orbital degeneracy, spin and valley polarized non-uniform states are allowed due to charge modulation in the orbital subspace. As we show these states only appear for $J > 2$ C2DEGs, and are the main focus of this paper.

The existence of these additional plateaus from spontaneously broken-symmetry ground state has already been

confirmed in suspended bilayer graphene samples and bilayer graphene on SiO₂/Si substrates¹³ as well as in graphene trilayers¹⁴. By applying an electric potential difference Δ_B (or *bias*) between the outermost layers (where the low-energy sites reside) of a graphene bilayer, one can control the population of electrons in each layer and open a gap $\Delta_{LL}(\Delta_B, B)$ between two adjacent orbital state which is a function of both Δ_B and the quantizing magnetic field B . The phase diagram of the C2DEG in the $\nu - \Delta_{LL}$ space has been studied for bilayer graphene and is very rich. States with spin and/or layer and/or orbital polarizations are possible^{10,12,15–17}. At $\nu = -1, 4$, the bias drives a series of transitions from an homogeneous state with finite orbital pseudospin to charge-density-wave states and crystal states where the orbital pseudospin rotates in space^{16,17}. Interestingly, a similar sequence of transitions has been observed in a thin film of the helical magnet Fe_{0.5}Co_{0.5}Si using Lorentz transmission electron microscopy^{18–20}. In that system, the phase transitions are induced by a transverse magnetic field. In the graphene bilayer, they are induced by Δ_B potential. The Hamiltonian of both systems are similar. In particular, they contain a Dzyaloshinsky-Moriya (DM) interaction²¹ which, in the bilayer, is entirely due to exchange interactions instead of from spin-orbit coupling.

In this paper, we study the quantum Hall ferromagnetic states of the C2DEG in trilayer graphene's zeroth LL. Assuming the layer and spin degrees of freedom are inactive¹², we only consider the orbital pseudospin at integer filling. This situation occurs at filling factors $\nu = -5, -4$ and $\nu = 4, 5$ for finite value of $|\Delta_{LL}|$ or at other filling factors in some specific range of Δ_{LL} . The phase diagram consists in a uniform phase which appears at large absolute values of Δ_{LL} where electrons occupy the lowest energy levels and there is no orbital coherence. Upon decreasing the value of $|\Delta_{LL}|$, the uniform state shows an instability in the pseudospin wave mode at finite wave vectors \mathbf{q} . This instability indicates, in principle, a transition to a unidirectional charge-density-wave state. We find, however, that this transition is preempted by a first-order transition to a crystal state with a vortex pseudospin texture. One remarkable result is that this crystal state in the trilayer exists at both positive and negative values of Δ_{LL} in contrast with the bilayer case where it is found for $\Delta_{LL} < 0$ only. The pseudospin texture of the crystal is more complex than in bilayer graphene since an electronic state in this system is described not by a CP¹ but by a CP² spinor. This spinor can be decomposed into three distinct pseudospin vectors. We show that our crystal has a vortex texture in each of these pseudospins but with different vorticities. We discuss some properties of the crystal and uniform phases in this article. In particular, we show that these states can be distinguished by their electromagnetic absorption spectrum.

Our paper is organized in the following way. In Sec. II, we review the effective two-band model Hamiltonian

for ABC-trilayer graphene. In Sec. III, we describe the Hartree-Fock and generalized random-phase formalism (GRPA) used to compute the energy and pseudospin textures of the different phases as well as their collective excitations. In Sec. IV, we explain our pseudospin representation for the various phases, define the electric dipole density and the formalism used to compute the electromagnetic absorption. The phase diagram of the C2DEG is presented in Sec. V. In Sec. VI we show that the uniform phase is unstable at a finite wave vector in some range of bias where the crystal state described in Sec. VII emerges. We discuss the properties of this crystal state in Sec. VIII and conclude in Sec. IX. Appendix A lists the values of the Coulomb exchange interactions at zero wave vector, Appendix B summarizes the Hartree-Fock and GRPA equations for the single and two-particle Green's functions and Appendix C gives the generators of the group SU(3).

II. ABC-TRILAYER GRAPHENE AS A C2DEG

In this section, we describe the low-energy effective Hamiltonian for the C2DEG in ABC-stacked trilayer graphene. Before we look at the specific details of ABC-stacked trilayer graphene lets us review the properties of C2DEGs⁸. The low-energy effective Hamiltonian of a chiral two-dimensional electron gas (C2DEG) can be written⁶ as

$$H_J = \xi^J v_F p_c \left(\frac{p}{p_c} \right)^J [\cos(J\theta) \sigma_x + \sin(J\theta) \sigma_y], \quad (1)$$

where σ_x, σ_y are Pauli matrices, p is the momentum of the electron, θ its angle with the x axis and J is the chirality index. The parameter $p_c = \gamma_1/v_0$ where γ_1 is the interlayer hopping energy between the two high-energy sites in adjacent planes and $v_F = 3c_0\gamma_0/2\hbar$ is the Fermi velocity with c_0 the separation between carbon atoms in a plane and γ_0 the intralayer hopping energy between two neighboring carbon atoms. This Hamiltonian operates in the space of a two-component wave functions Ψ_{\pm} describing electronic amplitudes on the two low-energy sites A and B . In the valley $K = (-2/3, 0)2\pi/a$, $\xi = -1$ and $\Psi_- = (\psi(A), \psi(B))$ whereas in the valley $K' = (2/3, 0)2\pi/a$, $\xi = +1$ and $\Psi_+ = (\psi(B), \psi(A))$. (For an introduction to the electronic properties of C2DEG's, see Ref. 8).

When a transverse magnetic field is applied to a C2DEG, the kinetic energy of the electrons is quantized into Landau levels with energies

$$E_{N,\xi} = \text{sgn}(N) \gamma_1 \xi \left(\frac{\sqrt{2}\hbar v_F}{\ell \gamma_1} \right)^J \sqrt{\prod_{i=0}^{J-1} (|N| - i)}, \quad (2)$$

where sgn is the signum function and $\ell = \sqrt{\hbar c/eB}$ is the magnetic length, $N = 0, \pm 1, \pm 2, \dots$ is the LL index. The LLs are 4-fold degenerate when counting valley and

spin degrees of freedom. The $N = 0$ LL is special since, including the valley and spin degrees of freedom, it is $4J$ -fold degenerate. The extra degeneracy comes from the fact that the eigenspinors in $N = 0$ which have the form $\{ \begin{pmatrix} 0 \\ h_{n,X}(\mathbf{r}) \end{pmatrix}, n = 0, 1, \dots, J-1 \}$ are degenerate (here, $h_{n,X}(\mathbf{r})$ represents the Landau-gauge wave functions of conventional 2DEGs given in Eq. (6) below). We refer to the index n as the *orbital* quantum number. The presence of wave functions with spatial structures that appear at different energies in the ordinary non-relativistic 2DEG model in the same degenerate manifold can create some terminological confusion. We will refer to the wave functions h_n as Landau level n orbitals and (as already anticipated) use upper case letter N to distinguish levels with different Landau-quantized band energies in the C2DEG model in a magnetic field.

The lattice structure of an ABC-stacked trilayer graphene (rhombohedral stacking) is shown in Fig. 1. Each layer has a honeycomb lattice of carbon atoms. The underlying Bravais lattice is a triangular lattice with a basis of two atoms denoted by A_m and B_m where m is the layer index. The triangular lattice constant is $a_0 = \sqrt{3}c_0$ where $c_0 = 1.42 \text{ \AA}$ is the distance between two neighboring carbon atoms. The Brillouin zone of the reciprocal lattice has two non-equivalent \mathbf{K} points that we take as $\mathbf{K}_{\pm} = \pm(2/3, 0)2\pi/a_0$ as indicated in the inset of Fig. 1. Each adjacent layer pair forms an AB-stacked bilayer with the upper B sublattice directly on top of the lower A sublattice. The upper A sublattice is above the center of a hexagonal plaquette of the layer below. Two adjacent layers are separated by a distance $d = 3.35 \text{ \AA}$.

The band structure of the ABC-stacked trilayer graphene has been studied in Refs.22,23. Near the valleys \mathbf{K}_{\pm} , it consists in three valence and three conduction bands as shown in Fig. 2. In the simplest model where only the nearest-neighbor intralayer $\gamma_0 \approx 3.16 \text{ eV}$ and interlayer hopping $\gamma_1 \approx 0.502 \text{ eV}$ are considered, the degenerate bands in the middle of Fig. 2 have a cubic dispersion. For undoped ABC-trilayer graphene, the valence bands are completely filled and the Fermi level lies at $E = 0$. The high-energy bands are separated by a gap γ_1 from the low-energy bands as shown in Fig. 2. The low-energy bands touch at the \mathbf{K}_{\pm} points while the other four bands cross at the energies $E = \pm\gamma_1$ above (below).

To study the low-energy behavior of the electrons, we use an effective two-band model which results from perturbation theory in v_0^3/γ_1^2 . This effective model can be derived for ABC-stacked trilayer^{22,23} starting from a coupled Dirac model, consistent with the stacking arrangement. In the basis of the low-energy sites (A_1, B_3) for the valley \mathbf{K}_+ and (B_3, A_1) for the valley \mathbf{K}_- , the resulting Hamiltonian, in the case where a perpendicular magnetic field is applied, is given by

$$H_{\xi}^0 = \begin{pmatrix} \Delta_{\xi} a a^{\dagger} & \xi \frac{v_0^3}{\gamma_1^2} a^3 \\ \xi \frac{v_0^3}{\gamma_1^2} (a^{\dagger})^3 & \Delta_{-\xi} a^{\dagger} a \end{pmatrix}, \quad (3)$$

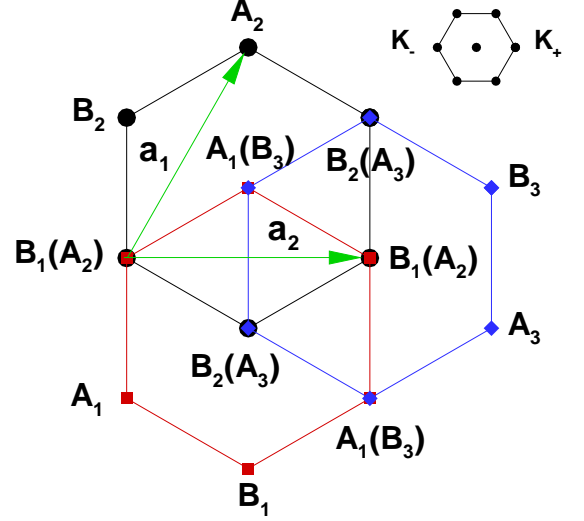


FIG. 1: (Color online) Lattice structure of an ABC-stacked graphene trilayer. The two non-equivalent sites of the honeycomb lattice in each plane are indicated by A_m and B_m , where m is the layer index. The two basis vectors of the underlying hexagonal Bravais lattice are $\mathbf{a}_1, \mathbf{a}_2$. The Brillouin zone of the hexagonal lattice with the two non-equivalent points \mathbf{K}_{\pm} is drawn in the top right corner of the figure.

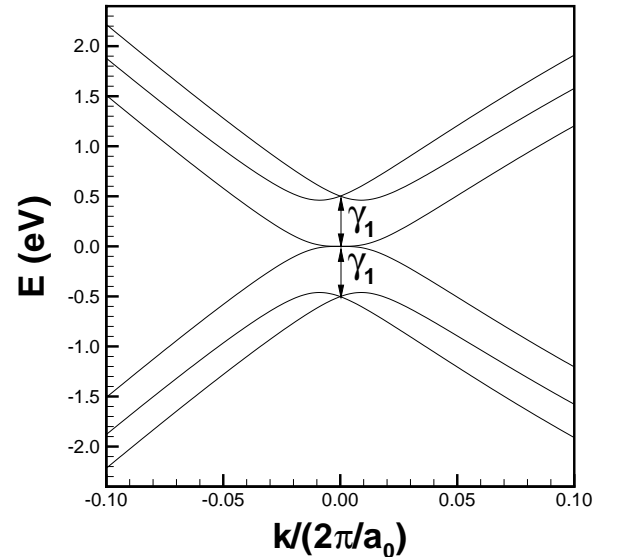


FIG. 2: Band structure of ABC-stacked trilayer graphene obtained from the tight-binding Hamiltonian by keeping the hopping parameters γ_0 and γ_1 only.

where

$$\Delta_\xi = \xi \frac{\Delta_B}{2} - \xi \beta^2 \frac{\Delta_B}{2}, \quad (4)$$

and $\beta = v_0/\gamma_1$. In Eq. (3), a, a^\dagger are the ladder operators for the Landau levels. The valley index is $\xi = \pm$ and we have defined $v_i = \sqrt{3/2}a_0\gamma_i/\ell$. In deriving, H_ξ^0 , we have taken into account a perpendicular electric field that forces a potential difference Δ_B (or *bias*) between the outermost layers. In a magnetic field, the low-energy bands of the full model are replaced by a set of Landau levels with energies, in the absence of bias, given by Eq. (2) with $J = 2$. These energies are independent of the guiding-center coordinate X so that each level has the usual degeneracy $N_\varphi = S/2\pi\ell^2$, where S is the area of the 2DEG. The three eigenspinor for the orbital states in $N = 0$ and in the Landau gauge $\mathbf{A} = (0, Bx, 0)$ are given by

$$\begin{pmatrix} 0 \\ h_{2,X}(\mathbf{r}) \end{pmatrix}, \begin{pmatrix} 0 \\ h_{1,X}(\mathbf{r}) \end{pmatrix}, \begin{pmatrix} 0 \\ h_{0,X}(\mathbf{r}) \end{pmatrix}, \quad (5)$$

where²⁴

$$h_{n,X}(\mathbf{r}) = \frac{1}{\sqrt{L_y}} e^{-iXy/\ell^2} \varphi_n(x - X), \quad (6)$$

are the wave functions in the Landau gauge with $\varphi_n(x)$ the wave functions of the one-dimensional harmonic oscillator.

A finite bias lifts this orbital degeneracy. The energies are proportional to Δ_B and are given as

$$E_{\xi,N=0,n}^0 = -\xi \frac{\Delta_B}{2} + n\xi\Delta_{LL}, \quad (7)$$

where

$$\Delta_{LL} = \beta^2 \frac{\Delta_B}{2}. \quad (8)$$

The correction Δ_{LL} is small compared to the bias. Indeed, if we use the values of the tight-binding parameters given in Ref. 23, we find $\beta^2 = 5.49 \times 10^{-3}B$ where B is the magnetic field in Tesla. One remarkable aspect of the energies of the orbital states is that the ordering of the energy levels in $N = 0$ is different in the two valleys. This property of the energy spectrum has profound consequences on the phase diagram of the C2DEG in trilayer graphene, as we will show in this paper.

Other remote inter-layer hopping parameters that have hitherto been neglected in our analysis can modify the energy spectrum. The hopping term γ_4 (which couples the low- and high-energy sites located on different layers) adds a finite correction $-2n\beta\nu_4$ to $E_{\xi,N=0,n}^0$ which is independent of the valley index and bias and scales linearly with the magnetic field. This correction lifts the degeneracy of the orbital states even at zero bias. We can include it in Δ_{LL} by redefining

$$\Delta_{LL} = \beta^2 \frac{\Delta_B}{2} - 2\xi\beta\nu_4. \quad (9)$$

In this paper, we take Δ_{LL} (not Δ_B) as the parameter that we vary to study the phase diagram of the C2DEG. Clearly, Δ_{LL} can be tuned by changing the bias or the magnetic field. It can have both positive and negative values. The maximal value of $|\Delta_{LL}|$ must be such that we stay within the limit of validity of the two-band model. This can be checked by comparing the band structure of the two-band model (Eqs. (7-9)) with that given by the full (six band) model with all hopping terms included. We have done this comparison and will report it elsewhere²⁵. Our conclusion is that there exists a range of bias where the two-band model is well-justified. This range increases with increasing magnetic field.

III. ORDER PARAMETERS AND COLLECTIVE EXCITATIONS

In the present work, we study the phases of the C2DEG when the Fermi level, filling factor and bias are such that the trilayer can reasonably be described by a three-level system in the $N = 0$ LL with level energies given by

$$E_n^0 = n\Delta_{LL}. \quad (10)$$

To do this, we must consider the valley and spin degrees of freedom to be frozen. This can occur, for example, at filling factors $\nu = -5, -4$ or at $\nu = 4, 5$ when the lower levels are fully filled and can be considered as inert. Also, when Coulomb interaction is included, the Zeeman gap is exchange-enhanced and, for the filling factors just mentioned, the ground states were shown to be spin polarized¹². Finally, interlayer coherence occurs only for very small bias $|\Delta_{LL}| \lesssim 0.001 e^2/\kappa\ell$ (we checked this numerically) so that, unless Δ_{LL} is close to zero, layer polarization can safely be assumed.

We denote by ν_n the filling factor of the orbital level n and by $\tilde{\nu}$ the filling factor of the three-level system. Our aim is to study the phase diagram of the C2DEG when $\tilde{\nu} = 1, 2$ (since $\tilde{\nu} = 3$ is trivial) as Δ_{LL} is varied.

To study the phase diagram, including both homogeneous and modulated states, we define the operators

$$\begin{aligned} \rho_{n,n'}(\mathbf{q}) &= \frac{1}{N_\varphi} \sum_{X,X'} e^{-\frac{i}{2}q_x(X+X')} \\ &\times c_{n,X}^\dagger c_{n',X'} \delta_{X,X'+q_y\ell^2}, \end{aligned} \quad (11)$$

where $N_\varphi = S/2\pi\ell^2$ is the Landau level degeneracy.

The Hartree-Fock Hamiltonian can then be written as

$$\begin{aligned} H_{HF} &= N_\varphi E_n^0 \rho_{n,n}(0) \\ &+ N_\varphi \sum_{\mathbf{q}} \overline{H_{n_1,n_2,n_3,n_4}}(\mathbf{q}) \langle \rho_{n_1,n_2}(-\mathbf{q}) \rangle \rho_{n_3,n_4}(\mathbf{q}) \\ &- N_\varphi \sum_{\mathbf{q}} X_{n_1,n_4,n_3,n_2}(\mathbf{q}) \langle \rho_{n_1;n_2}(-\mathbf{q}) \rangle \rho_{n_3,n_4}(\mathbf{q}), \end{aligned} \quad (12)$$

where repeated indices are summed over. In deriving Eq. (12), we have taken into account a neutralizing positive background so that the $\mathbf{q} = 0$ contribution is absent from the Hartree term. This is indicated by a bar over the summation.

The Hartree and Fock interactions are defined by

$$H_{n_1, n_2, n_3, n_4}(\mathbf{q}) = \left(\frac{e^2}{\kappa \ell} \right) \frac{1}{q \ell} K_{n_1, n_2}(\mathbf{q}) K_{n_3, n_4}(-\mathbf{q}) \quad (13)$$

$$X_{n_1, n_2, n_3, n_4}(\mathbf{q}) = \int \frac{d\mathbf{p} \ell^2}{2\pi} H_{n_1, n_2, n_3, n_4}(\mathbf{p}) e^{i\mathbf{q} \times \mathbf{p} \ell^2} \quad (14)$$

The Coulomb energy $e^2/\kappa \ell = 56.2\sqrt{B}$ meV with B in Tesla and $\kappa = 1$. The Fock interactions $X_{n_1, n_2, n_3, n_4}(\mathbf{q} = 0)$ are listed in Appendix A.

The form factors which appear in H and X are given by

$$K_{n_1, n_2}(\mathbf{q}) = \begin{cases} F_{n_1, n_2}(\mathbf{q}) & \text{if } n_1 \geq n_2 \\ [F_{n_2, n_1}(-\mathbf{q})]^* & \text{if } n_1 \leq n_2 \end{cases}, \quad (15)$$

with

$$F_{n, n'}(\mathbf{q}) = \sqrt{\frac{n!}{n'}} \left(\frac{(q_y + i q_x) \ell}{\sqrt{2}} \right)^{n-n'} \times e^{-\frac{q^2 \ell^2}{4}} L_{n'}^{n-n'} \left(\frac{q^2 \ell^2}{2} \right). \quad (16)$$

They capture the character of the different orbital states.

Finally, the Hartree-Fock energy per electron is given by

$$\begin{aligned} \frac{E_{HF}}{N_e} &= \frac{1}{\tilde{\nu}} E_n^0 \langle \rho_{n, n}(0) \rangle \\ &+ \frac{1}{2\tilde{\nu}} \sum_{\mathbf{q}} \overline{H}_{n_1, n_2, n_3, n_4}(\mathbf{q}) \langle \rho_{n_1, n_2}(-\mathbf{q}) \rangle \langle \rho_{n_3, n_4}(\mathbf{q}) \rangle \\ &- \frac{1}{2\tilde{\nu}} \sum_{\mathbf{q}} X_{n_1, n_4, n_3, n_2}(\mathbf{q}) \langle \rho_{n_1, n_2}(-\mathbf{q}) \rangle \langle \rho_{n_3, n_4}(\mathbf{q}) \rangle, \end{aligned} \quad (17)$$

where N_e is the number of electrons in the C2DEG.

The order parameters of the orbital phases are obtained from the single-particle Matsubara Green's function

$$G_{n_1, n_2}(X, X', \tau) = - \left\langle T_\tau c_{n_1, X}(\tau) c_{n_2, X'}^\dagger(0) \right\rangle, \quad (18)$$

where T_τ is the imaginary time ordering operator and $c_{n, X}^\dagger$ creates an electron in orbital n with guiding-center X .

If we define the Fourier transform of the single-particle Green's function as

$$\begin{aligned} G_{n_1, n_2}(\mathbf{q}, \tau) &= \frac{1}{N_\varphi} \sum_{X, X'} e^{-\frac{i}{2} q_x (X + X')} \\ &\times \delta_{X, X' - q_y \ell^2} G_{n_1, n_2}(X, X', \tau), \end{aligned} \quad (19)$$

then the order parameters of the coherent phases are simply

$$\langle \rho_{n_1, n_2}(\mathbf{q}) \rangle = G_{n_2, n_1}(\mathbf{q}, \tau = 0^-). \quad (20)$$

The equation of motion for the Green's function in the Hartree-Fock approximation is given in Appendix B. This equation leads to the sum rule (at $T = 0$ K)

$$\sum_{\mathbf{q}} \sum_{n_2} |\langle \rho_{n_1, n_2}(\mathbf{q}) \rangle|^2 = \langle \rho_{n_1, n_1}(0) \rangle. \quad (21)$$

By definition, we also have

$$\langle \rho_{n, n}(0) \rangle = \nu_n. \quad (22)$$

To study the collective excitations, we compute the two-particle Green's function

$$\begin{aligned} \chi_{n_1, n_2, n_3, n_4}(\mathbf{q}, \mathbf{q}'; \tau) &= -N_\varphi \langle T_\tau \rho_{n_1, n_2}(\mathbf{q}, \tau) \rho_{n_3, n_4}(-\mathbf{q}', 0) \rangle \\ &+ N_\varphi \langle \rho_{n_1, n_2}(\mathbf{q}) \rangle \langle \rho_{n_3, n_4}(-\mathbf{q}') \rangle \end{aligned} \quad (23)$$

in the generalized random-phase approximation²⁶ (GRPA). The resulting set of equations is given in Appendix B. The collective excitations are given by the poles of the retarded Green's function $\chi_{n_1, n_2, n_3, n_4}^{(R)}(\mathbf{q}, \mathbf{q}, \omega) = \chi_{n_1, n_2, n_3, n_4}(\mathbf{q}, \mathbf{q}; i\Omega_n \rightarrow \omega + i\delta)$. To derive the dispersion relations, we follow these poles as the wave vector \mathbf{q} is varied in the Brillouin zone.

IV. DESCRIPTION OF THE ORBITAL-COHERENT PHASES

A. Pseudospin representation

An electronic state in our three-state model can be created by the spinor field

$$\Phi^\dagger(\mathbf{r}) = \begin{pmatrix} \Psi_0^\dagger(\mathbf{r}) \\ \Psi_1^\dagger(\mathbf{r}) \\ \Psi_2^\dagger(\mathbf{r}) \end{pmatrix}, \quad (24)$$

where $\Psi_n^\dagger(\mathbf{r}) = \sum_X h_{n, X}^*(\mathbf{r}) c_{n, X}^\dagger$.

Using the eight infinitesimal generators T_a (with $a = 1, 2, \dots, 8$) of SU(3) (see Appendix C), we can define the eight real fields

$$\tilde{F}_a(\mathbf{r}) = \Phi^\dagger(\mathbf{r}) T_a \Phi(\mathbf{r}) \quad (25)$$

with the Fourier transforms

$$\tilde{F}_a(\mathbf{q}) = \int d\mathbf{r} e^{-i\mathbf{q} \cdot \mathbf{r}} \Phi^\dagger(\mathbf{r}) T_a \Phi(\mathbf{r}). \quad (26)$$

With $a = 1$, we get

$$\tilde{F}_1(\mathbf{q}) = \frac{1}{2} [N_\phi K_{0,1}(-\mathbf{q}) \rho_{0,1}(\mathbf{q}) + N_\phi K_{1,0}(-\mathbf{q}) \rho_{1,0}(\mathbf{q})]. \quad (27)$$

We describe the three-level system by three pseudospins²⁷ $1/2$. We associate spin up(down) with level $n = i(j)$ to get the spin (i, j) system. We take $(i, j) = (0, 1); (1, 2); (0, 2)$. We suppress the orbital-dependent part of the form factor and keep only the factor $\beta_q = e^{-\frac{q^2 \ell^2}{4}}$ in $K_{i,j}(\mathbf{q})$ for all i, j . Eq. (27), for example, becomes

$$\tilde{F}_1(\mathbf{q}) = \beta_q \rho_x^{(0,1)}(\mathbf{q}), \quad (28)$$

where $\rho_x^{(i,j)} = \frac{1}{2}(\rho_{i,j} + \rho_{j,i})$. The other components are listed in Appendix C. We also add to these fields the “densities”

$$\rho_i(\mathbf{q}) = \beta_q \rho_{i,i}(\mathbf{q}), \quad (29)$$

with $i = 0, 1, 2$.

The eight real fields $F_i(\mathbf{r})$ (the Fourier transforms of $F_i(\mathbf{q})$) provide a complete description of each phase studied in this paper.

B. Dipole density

The total electronic density is given by

$$n(\mathbf{r}) = \sum_{i,j} \Psi_i^\dagger(\mathbf{r}) \Psi_j(\mathbf{r}). \quad (30)$$

Its Fourier transform is

$$n(\mathbf{q}) = N_\varphi \sum_{i,j=0}^2 K_{i,j}(-\mathbf{q}) \rho_{i,j}(\mathbf{q}). \quad (31)$$

An external electric field, $\mathbf{E}_{ext}(\mathbf{r}) = -\nabla \phi_{ext}(\mathbf{r})$, couples to the density through a term

$$H_{ext} = -\frac{e}{S} \sum_{\mathbf{q}} n(-\mathbf{q}) \phi_{ext}(\mathbf{q}), \quad (32)$$

in the Hamiltonian where

$$\phi_{ext}(\mathbf{r}) = \frac{1}{S} \sum_{\mathbf{q}} \phi_{ext}(\mathbf{q}) e^{i\mathbf{q} \cdot \mathbf{r}}. \quad (33)$$

Using the definition of the form factors $K_{i,j}(\mathbf{q})$ given in Eq. (15), the coupling H_{ext} can be written as

$$H_{ext} = \int d\mathbf{r} \rho_{TOT}(\mathbf{r}) \phi(\mathbf{r}) - \int d\mathbf{r} (\mathbf{d}(\mathbf{r}) \cdot \mathbf{E}(\mathbf{r})), \quad (34)$$

where

$$\rho_{TOT}(\mathbf{q}) = -e \frac{1}{S} \sum_{i=0}^2 N_\varphi e^{-q^2 \ell^2 / 4} e \rho_{i,i}(\mathbf{q}), \quad (35)$$

and we can define the dipole operators

$$d_x(\mathbf{q}) = -\gamma(\mathbf{q}) [\rho_x^{(0,1)}(\mathbf{q}) + \alpha(\mathbf{q}) \rho_x^{(1,2)}(\mathbf{q})], \quad (36)$$

$$d_y(\mathbf{q}) = \gamma(\mathbf{q}) [\rho_y^{(0,1)}(\mathbf{q}) + \alpha(\mathbf{q}) \rho_y^{(1,2)}(\mathbf{q})], \quad (37)$$

with $\alpha(\mathbf{q}) = \sqrt{2}(1 - q^2 \ell^2 / 4)$ and $\gamma(\mathbf{q}) = \sqrt{2} N_\varphi e \ell e^{-q^2 \ell^2 / 4}$.

In the phases studied in this paper, $\langle \rho_{TOT}(\mathbf{r}) \rangle$ is always uniform i.e. $\sum_{i=0}^2 \langle \rho_{i,i}(\mathbf{q}) \rangle = \tilde{\nu} \delta_{\mathbf{q},0}$ for $\tilde{\nu} = 1, 2$. It follows that we can ignore the first term in H_{ext} in Eq. (35) and the coupling with the external electric field is simply

$$H_{ext} = - \int d\mathbf{r} (\mathbf{d}(\mathbf{r}) \cdot \mathbf{E}(\mathbf{r})), \quad (38)$$

where $\mathbf{d}(\mathbf{r})$ can be interpreted as a density of electric dipoles²⁸.

In the absence of Coulomb interaction, the time variation of the total dipole moment is given by

$$\begin{aligned} i\hbar \frac{d}{dt} \mathbf{d}(0) &= -[H_{HF}^0, \mathbf{d}(0)] \\ &= i\Delta_{LL} \hat{\mathbf{z}} \times \mathbf{d}(0), \end{aligned} \quad (39)$$

where

$$H_{HF}^0 = N_\varphi [\Delta_{LL} \rho_{1,1}(0) + 2\Delta_{LL} \rho_{2,2}(0)], \quad (40)$$

so that the dipoles oscillate at the frequency

$$\omega_{dip} = \Delta_{LL} / \hbar. \quad (41)$$

We can define a dipolar current density by

$$\mathbf{J}^{dip} = \frac{d}{dt} \mathbf{d}(0). \quad (42)$$

C. Optical absorption

The total current in the 2DEG is given by

$$\mathbf{J} = \int d\mathbf{r} \frac{1}{2} [(\Psi^\dagger(\mathbf{r}) \mathbf{j} \Psi(\mathbf{r})) + (\mathbf{j} \Psi(\mathbf{r}))^\dagger \Psi(\mathbf{r})], \quad (43)$$

where

$$\mathbf{j} = -c \frac{\partial H^0}{\partial \mathbf{A}^e} \Big|_{\mathbf{A}^e \rightarrow 0}, \quad (44)$$

with \mathbf{A}^e the vector potential of the external electromagnetic field and H^0 is the Hamiltonian of the two-band model. We find

$$J_x = -4\Xi [\rho_y^{(0,1)}(0) + \sqrt{2} \rho_y^{(1,2)}(0)], \quad (45)$$

$$J_y = -4\Xi [\rho_x^{(0,1)}(0) + \sqrt{2} \rho_x^{(1,2)}(0)], \quad (46)$$

with the constant

$$\Xi = N_\phi \frac{1}{2\sqrt{2}} \frac{e\ell}{\hbar} \Delta_{LL}. \quad (47)$$

The total current²⁹ given by Eqs. (45-46) is nothing but the dipolar current defined in Eq. (42) above i.e. $\mathbf{J} = \mathbf{J}^{dip}$.

The optical absorption per unit surface from an electromagnetic wave $\mathbf{E} = E_0 \hat{\mathbf{e}}_\alpha e^{i\omega t}$ (with $\alpha = x, y$ and we define $\bar{\alpha} = x$ if $\alpha = y$ and $\bar{\alpha} = y$ if $\alpha = x$) is obtained from the retarded current-current response function

$$\begin{aligned} P_\alpha(\omega) &= -\frac{1}{\hbar} \Im \left[\frac{\chi_{J_\alpha, J_\alpha}^{ret}(\omega)}{\omega + i\delta} \right] E_0^2 \\ &= -\frac{2}{\hbar} \left(\frac{eE_0 \Delta_{LL}}{\hbar} \right)^2 \text{Im} \left[\frac{\chi_{\bar{\alpha}, \bar{\alpha}}(0, \omega)}{\omega + i\delta} \right], \end{aligned} \quad (48)$$

where the retarded current response function is obtained from the time-ordered two-particle Green's function

$$\chi_{J_\alpha, J_\beta}(\tau) = -\langle T J_\alpha(\tau) J_\beta(0) \rangle, \quad (49)$$

with

$$\chi_{\alpha, \beta}(0, \tau) = -\langle T \rho_\alpha(0, \tau) \rho_\beta(0, 0) \rangle \quad (50)$$

and

$$\rho_\alpha(0, \tau) = \rho_\alpha^{(0,1)}(0, \tau) + \sqrt{2} \rho_\alpha^{(1,2)}(0, \tau). \quad (51)$$

V. PHASE DIAGRAM OF THE C2DEG

The ground state in the ABC-trilayer graphene can be classified in terms of translationally invariant (uniform) states or non-translationally invariant (non-uniform) states. One important distinction to note is that any non-uniform state in graphene would otherwise be either spin or valley density waves. However, for spin and valley polarized $J \geq 2$ C2DEGs, non-uniform states are generically allowed due to charge modulation in the orbital subspace. Both states have different experimental signatures: uniform states exhibit Hall conductivity whereas if the topmost occupied LL has a crystal-like state or unidirectional charge-density-wave, it will either be insulating or exhibit anisotropic conductivity. In the case of crystal-like states discussed here, which will likely be pinned by disorder, the Hall conductivity σ_{xy} will be at a value corresponding to the *adjacent* interaction driven integer quantum Hall plateau as we will discuss.

In our study of the phase diagram, we consider the following states:

1. A coherent uniform state (CUP). In this state, the only allowed order parameters are $\langle \rho_{n,m}(\mathbf{q} = 0) \rangle$. The state of each electron is described by the CP² spinor (a_0, a_1, a_2) (where a_i 's are complex numbers satisfying $\sum_n |a_n|^2 = 1$) so that an electron

at guiding-center X is in a linear combination of the three orbital states. This combination is the same for all electrons. The CUP ground state is written as

$$|\Psi\rangle_{CUP} = \prod_X \left[\sum_{n=0}^2 a_n c_{n,X}^\dagger \right] |0\rangle \quad (52)$$

which gives

$$\langle \rho_{n,m}(\mathbf{q} = 0) \rangle = a_n^* a_m. \quad (53)$$

Due to particle-hole symmetry the ground state for $\tilde{\nu} = 2$ can be described as a filled level of holes on a vacuum state consisting of the three levels filled with electrons. The CP² spinor (a_0, a_1, a_2) also applies to a hole state if $c_{nX}^\dagger \rightarrow b_{nX}^\dagger$ (where b_{nX}^\dagger is a hole creation operator). The CUP phase is possible at negative bias because the system can then reduce its kinetic energy by populating the levels $n = 1, 2$ that are below level $n = 0$ in energy. This, however, increases the exchange energy because the Coulomb exchange terms satisfy $X_{0,0,0,0}(0) > X_{1,1,1,1}(0) > X_{2,2,2,2}(0)$ (see Appendix A). In consequence, there is an optimal population of the levels that minimizes the total energy.

2. An incoherent uniform phase (IUP). In this case, the only allowed order parameters are $\langle \rho_{n,n}(\mathbf{q} = 0) \rangle$ and the first ($\tilde{\nu} = 1$) or first two ($\tilde{\nu} = 2$) lowest-lying orbital states are fully filled so that all coherences $a_n^* a_m$ ($n \neq m$) are zero. For $\tilde{\nu} = 1$, we have in this limit $a_0 = 1$ when $\Delta_{LL} > 0$ and $a_2 = 1$ when $\Delta_{LL} < 0$. (It is just the opposite for the hole spinor when $\tilde{\nu} = 2$.)
3. A coherent charge-density-wave phase (CCDWP). This state is modulated in one direction only and the allowed order parameters are $\langle \rho_{n,m}(p\mathbf{q}_0) \rangle$ where $p = 0, \pm 1, \pm 2, \dots$ and \mathbf{q}_0 is the wave vector of the CCDWS. The ground state is simply obtained by letting $a_n \rightarrow a_n(X)$ in Eq. (52).
4. A coherent crystal phase (CCP). In this non-uniform state, all order parameters $\{\langle \rho_{n,m}(\mathbf{G}) \rangle\}$ are allowed where $\{\mathbf{G}\}$ are the reciprocal lattice vectors of the Bravais lattice of the crystal. We have considered a triangular and a square lattice with one electron per unit cell.

Note that in all of these states, the "density" $\langle \rho(\mathbf{r}) \rangle = \sum_n \langle \rho_{n,n}(\mathbf{r}) \rangle$ is a constant in space. The real density $\langle n(\mathbf{r}) \rangle$ as defined in Eq. (30) is modulated in space in the CCDWP and CCP.

Our Hartree-Fock numerical calculations for the phase diagram of the C2DEG is shown in Table 1. The CUP and CCDWP are never the ground state. The ground state is an IUP for large value of $|\Delta_{LL}|$ and a CCP (with a triangular lattice) in between. The transitions from the IUP to the crystal state are first order.

Phase	Δ_{LL}
IUP in $n = 2$	$\Delta_{LL} < -0.31(-0.34) e^2/\kappa\ell$
CCP	$-0.31(-0.34) e^2/\kappa\ell < \Delta_{LL} < 0.09(0.03) e^2/\kappa\ell$
IUP in $n = 0$	$\Delta_{LL} > 0.09(0.03) e^2/\kappa\ell$

TABLE I: Phase diagram including the uniform and crystal phases for $\tilde{\nu} = 1$. The numbers in parenthesis are for $\tilde{\nu} = 2$.

We discuss the crystal state in more details in the next section. We point out here, however, that the presence in the phase diagram of a crystal state at positive value of Δ_{LL} is something specific to trilayer graphene or other C2DEGS with $J > 2$ as discussed in Sec. VII A below.

VI. PROPERTIES OF THE UNIFORM PHASES

Even though the CUP is not the ground state in trilayer graphene, we would like to give a brief description some of its properties. In particular, it shows an instability to a CCDW state that is, in the case of the trilayer, preempted by the crystal phase. Comparing the energies of the IUP and CUP in the HFA, we find that the CUP has lower energy than the IUP in the range of bias $\Delta_{LL} \in [\Delta_{LL}^{(*)}, 0]$ where $\Delta_{LL}^{(*)} = -0.29e^2/\kappa\ell$ for $\tilde{\nu} = 1$ and $\Delta_{LL}^{(*)} = -0.24e^2/\kappa\ell$ for $\tilde{\nu} = 2$.

The ground-state energy per electron in a uniform phase is given by

$$\begin{aligned}
\frac{E_{CUP}}{N_e} = & \frac{1}{\tilde{\nu}} [\Delta_{LL} \langle \rho_{1,1} \rangle + 2\Delta_{LL} \langle \rho_{2,2} \rangle] \\
& - \frac{1}{2\tilde{\nu}} [X_{0,0,0,0} \langle \rho_{0,0} \rangle^2 + X_{1,1,1,1} \langle \rho_{1,1} \rangle^2 + X_{2,2,2,2} \langle \rho_{2,2} \rangle^2] \\
& - \frac{1}{\tilde{\nu}} [X_{0,1,1,0} \langle \rho_{0,0} \rangle \langle \rho_{1,1} \rangle + X_{0,2,2,0} \langle \rho_{0,0} \rangle \langle \rho_{2,2} \rangle] \\
& - \frac{1}{\tilde{\nu}} [X_{1,2,2,1} \langle \rho_{1,1} \rangle \langle \rho_{2,2} \rangle] \\
& - \frac{1}{\tilde{\nu}} [X_{0,0,1,1} |\langle \rho_{0,1} \rangle|^2 + X_{0,0,2,2} |\langle \rho_{0,2} \rangle|^2 + X_{1,1,2,2} |\langle \rho_{1,2} \rangle|^2] \\
& - \frac{1}{\tilde{\nu}} [X_{0,1,2,1} \langle \rho_{0,1} \rangle \langle \rho_{2,1} \rangle + X_{1,0,1,2} \langle \rho_{1,2} \rangle \langle \rho_{1,0} \rangle]
\end{aligned} \quad (54)$$

where all $\langle \rho_{i,j} \rangle$'s and the interactions $X_{i,j,k,l}$ are evaluated at $\mathbf{q} = 0$. Note that if we make a local gauge transformation of the CP² spinor i.e. $a_i(X) \rightarrow a_i e^{i\Lambda(X)}$, the energy E_{CUP} is unchanged. This U(1) gauge invariance is necessary to define the CP² spinor³⁰. Fig. 3 shows the occupation of the levels in both phases (IUP and CUP) for filling factors $\tilde{\nu} = 1, 2$.

One possible parametrization of a CP² spinor is given by³¹

$$\begin{pmatrix} \cos \theta \\ e^{i\alpha} \sin \theta \cos \varphi \\ e^{i(\beta+\alpha)} \sin \theta \sin \varphi \end{pmatrix}. \quad (55)$$

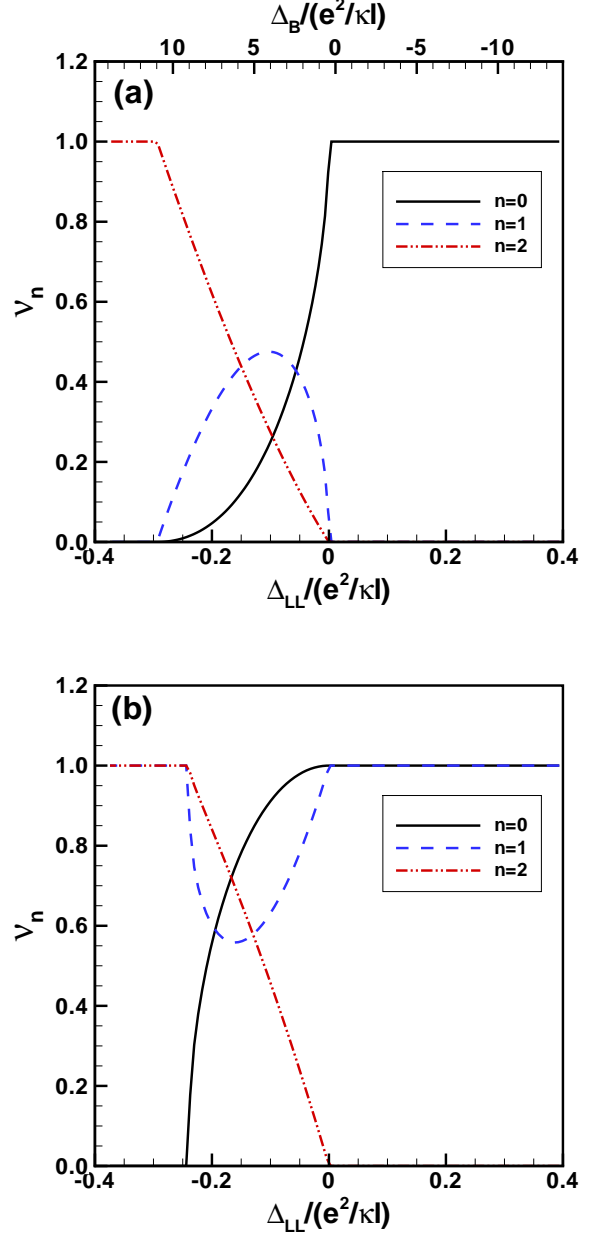


FIG. 3: (Color online) Occupation of the orbital levels in the incoherent ($\Delta_{LL} \geq 0$) and coherent ($\Delta_{LL} \leq 0$) uniform phases for $B = 10$ T as a function of the bare gap Δ_{LL} . (a) $\tilde{\nu} = 1$ and (b) $\tilde{\nu} = 2$.

The first four lines on the right hand side of Eq. (54) are independent of the angles α and β while the two terms in the last line depend on $\cos(\alpha - \beta)$. We have verified numerically that the ground state energy is minimized when $\alpha = \beta$ and that it is independent of the choice of α . The CUP thus has a broken U(1) symmetry and supports a Goldstone mode. This is confirmed by our GRPA calculation which also shows that the dispersion of this mode is highly anisotropic. The CUP in a graphene bilayer has similar properties as reported in Ref. 16 where

the origin of the anisotropy is discussed.

By contrast, the lowest-energy mode in the IUP is gapped and has an isotropic dispersion. This gap can be calculated analytically from the GRPA equations. We find

$$\omega_{IUP}(\mathbf{q}=0) = \begin{cases} \Delta_{LL}, & \text{if } \tilde{\nu} = 1, \Delta_{LL} \geq 0 \\ -\Delta_{LL} - \frac{15}{64} \sqrt{\frac{\pi}{2}} \left(\frac{e^2}{\kappa\ell} \right), & \text{if } \tilde{\nu} = 1, \Delta_{LL} \leq 0 \\ \Delta_{LL}, & \text{if } \tilde{\nu} = 2, \Delta_{LL} \geq 0 \\ -\Delta_{LL} - \frac{3}{16} \sqrt{\frac{\pi}{2}} \left(\frac{e^2}{\kappa\ell} \right), & \text{if } \tilde{\nu} = 2, \Delta_{LL} \leq 0 \end{cases} \quad (56)$$

The critical bias $\Delta_{LL}^{(*)}$ for the transition from the IUP to the CUP is given by the condition $\omega_{IUP}(\mathbf{q}=0) = 0$. The frequency $\omega_{IUP}(\mathbf{q}=0)$ is however positive in the region where the IUP is the ground state according to Table 1. This frequency is measurable in electromagnetic absorption experiments. We come back to this point in Sec. VIII.

The dispersion of the lowest-energy mode in the IUP and CUP becomes unstable at a finite value of \mathbf{q} in some range of bias $\Delta_{LL} \in [\Delta_{LL}^{(1)}, \Delta_{LL}^{(2)}]$. Fig. 4 shows the situation for $\tilde{\nu} = 1$. In this case, the IUP is unstable for $q\ell \approx 2$ at $\Delta_{LL}^{(2)} = 0.016 e^2/\kappa\ell$ while the CUP is unstable for $q_y\ell \approx -2$ and $q_y\ell \approx -3$ at $\Delta_{LL}^{(1)} = -0.25 e^2/\kappa\ell$. The direction in \mathbf{q} -space of the instability is related to the orientation of the electric dipoles present in the CUP. The instability in $\omega(\mathbf{q})$ occurs in the direction $\hat{\mathbf{q}} = \hat{\mathbf{z}} \times \hat{\mathbf{d}}(\mathbf{r})$ as in the bilayer case¹⁶. The dispersions at these two biases are plotted in Fig. 5. For filling factor $\tilde{\nu} = 2$, it is the IUP at *negative* Δ_{LL} that becomes unstable for $\Delta_{LL} \geq \Delta_{LL}^{(1)} = -0.27 e^2/\kappa\ell$ and the instability persists well into the CUP until $\Delta_{LL}^{(2)} = -0.036 e^2/\kappa\ell$. The system is stable for $\Delta_{LL} \geq \Delta_{LL}^{(2)}$.

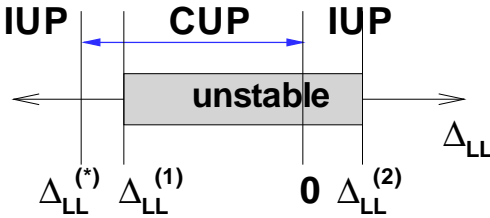


FIG. 4: (Color online) Phase diagram at $\tilde{\nu} = 1$. The incoherent uniform phase (IUP) occurs for $\Delta_{LL} \geq 0$ and for $\Delta_{LL} \leq \Delta_{LL}^{(*)}$. In between these two biases, the system is in a coherent uniform phase (CUP) in the HFA. In the GRPA, the collective excitations show that the uniform phases are unstable between $\Delta_{LL}^{(1)}$ and $\Delta_{LL}^{(2)}$.

The instability at a finite wave vector suggests that both uniform phases are unstable towards the formation

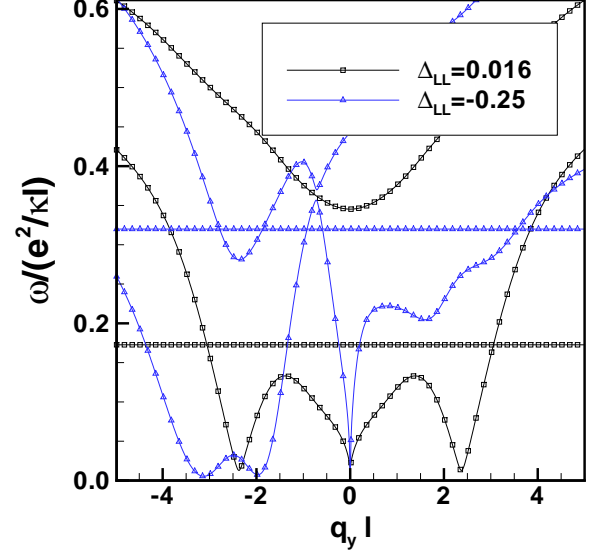


FIG. 5: (Color online) Dispersion relation of the collective modes in the uniform phases near the instability points $\Delta_{LL}^{(1)} = -0.25 e^2/\kappa\ell$ (CUP) and $\Delta_{LL}^{(2)} = 0.016 e^2/\kappa\ell$ (IUP) defined in Fig.4.

of some kind of charge-density-wave state. Some of us discussed this instability in Ref.12. For negative value of Δ_{LL} , this is not surprising. The same situation occurs in bilayer graphene^{16,17}. The instability for *positive* value of Δ_{LL} is unexpected, however, and does not occur in bilayer graphene¹⁰.

VII. CRYSTAL STATE WITH ORBITAL COHERENCE

In the HFA, we find that the instability towards the CDW state is preempted by the formation of a coherent crystal phase (CCP) with a triangular lattice. This electron crystal has one electron ($\tilde{\nu} = 1$) or one hole ($\tilde{\nu} = 2$) per site so that the lattice constant is $a_0/\ell = \sqrt{2\pi/\sqrt{3}/2}$ in both cases. The real density $n(\mathbf{r})$ is modulated in space but not the "density" $\langle \rho(\mathbf{r}) \rangle = \sum_n \langle \rho_{n,n}(\mathbf{r}) \rangle$ which is a constant. At integer filling, this is possible because in our system, the electrons can be distributed in more than one orbital states. Every electron in the CCP is in a linear superposition of the three orbital states as in the CUP but also in a superposition of guiding center states X . All order parameters $\langle \rho_{n,m}(\mathbf{G}) \rangle$ are finite where $\{\mathbf{G}\}$ are the reciprocal lattice vectors of the crystal. We choose $|\mathbf{G}|$ big enough in the numerical calculation to insure that the crystal energy converges to the required accuracy. We show in Fig. 6 the filling factors ν_n of the orbital states as well as the cohesive energy of the crystal. This energy is quite large, of the order of $0.04 e^2/\kappa\ell \approx 7 \text{ meV} \approx 80 \text{ K}$

at $B = 10$ T and for $\kappa = 1$. Hence, this state should be quite robust against thermal fluctuations and disorder.

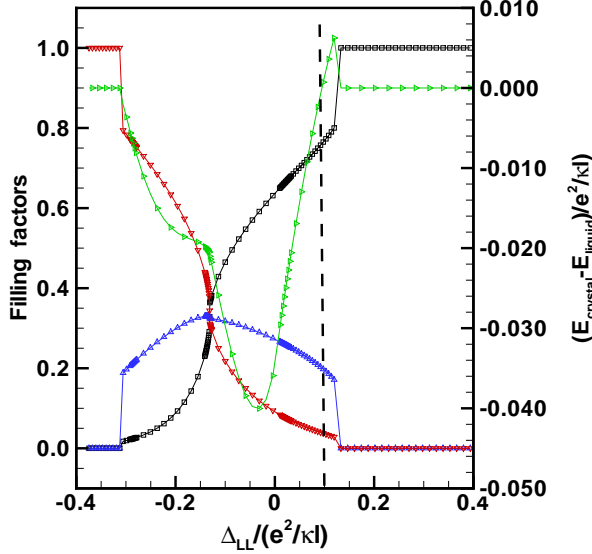


FIG. 6: (Color online) Filling factors (left y axis) of the orbital levels $n = 0$ (squares), $n = 1$ (delta), and $n = 2$ (nabla) in the crystal states for $\tilde{\nu} = 1$ and $B = 10$ T. The difference in energy between the crystal and the uniform states is shown by the green curve with the right triangles (right y axis). The dashed vertical line indicates the point where the uniform state is lower in energy than the crystal state for Δ_{LL} positive.

We show in Fig. 7 the electronic density $n(\mathbf{r})$ and the full SU(3) pseudospin representation of the crystal state for $\tilde{\nu} = 1$ at $B = 10$ T. We have chosen $\Delta_{LL} = 0$ in this figure, but the textures do not change much as Δ_{LL} is varied. We remark that the fields $\tilde{F}_a(\mathbf{r})$ defined in Eq. (28) represent pseudospin *densities*. These are not bounded. In particular, they are not normalized in Fig. 7. We find that for the three pseudospin fields, $\langle \rho_z^{(i,j)}(\mathbf{r}) \rangle \gg \langle \rho_x^{(i,j)}(\mathbf{r}) \rangle, \langle \rho_y^{(i,j)}(\mathbf{r}) \rangle$ so that the pseudospin are almost completely polarized in the direction of the z axis or opposite to it. The in-plane component of the pseudospin vectors (and so the interorbital coherence) is small. There is however a small clockwise rotation of the in-plane component of the pseudospins in the $x-y$ plane around each lattice site. For $(i,j) = (0,1)$ and $(1,2)$ the rotation of the pseudospins is of 2π while for $(0,2)$ the pseudospins rotate by 4π .

We conjecture that the interesting pseudospin texture around each lattice site can be assigned a topological charge. The minimal CP² sigma model is known to support skyrmion solutions³¹. In our case, where multiple orbitals are considered, the energy of long-wavelength deformations contains much more terms than the minimal CP² sigma model. In particular, it involves multiple pseudospin stuffiness. Nevertheless, we believe that

finite energy excitations should fall into different topological sectors even in this case. More work is needed, however, to confirm our conjecture.

A more physical quantity to represent graphically is the dipole density defined in Eqs. (36,37). It is shown in Fig. 8 for filling factors $\tilde{\nu} = 1, 2$. The vector field of the dipole density has also a vortex structure around each lattice site. The dipole vectors rotate by 2π in both cases.

A. Absence of the crystal state in bilayer graphene

As shown in Fig. 9, the effective interactions $H_{n_1, n_2, n_3, n_4}(\mathbf{q}) - X_{n_1, n_4, n_3, n_2}(\mathbf{q})$ which appears in the Hartree-Fock energy favor the formation of a CCDWP or CCP state because most of them take their minimal value at a finite wave vector. Because the filling factor is an integer, the system must put some of the electrons in the higher-energy orbital states in order to produce a density modulation. These modulations increases the Hartree energy of the system and, in the case where $\Delta_{LL} > 0$, the occupation of the higher-energy levels increases the bias energy. Nevertheless, the crystal state is favored in the trilayer because these costs are more than compensated by the gain in exchange energy as shown in Fig. 10.

In the Bernal-stacked bilayer, the Hartree-Fock equation admits a crystal solution for $\Delta_{LL} > 0$ but its total energy is greater than that of the IUP (see 10 (b)). We believe that the crystal energy in the bilayer case is not optimal because of the following reason. The effective interactions are not monotonous as shown in Fig. 9. At the value \mathbf{q}_0 where the energy is minimal, the particular effective interaction $H_{n,n,n,n}(\mathbf{q}_0) - X_{n,n,n,n}(\mathbf{q}_0)$ is smaller for $n = 0$. At larger value of \mathbf{q} , it is the opposite i.e. the interaction is smaller for $n = 2$. (The ordering in energy of the interaction $H_{n_1, n_2, n_3, n_4}(\mathbf{q}) - X_{n_1, n_4, n_3, n_2}(\mathbf{q})$ depends very much on the indices n_1, \dots, n_4). In a crystal, $\langle \rho_{n_1, n_2}(\mathbf{G}) \rangle$ is non zero for an infinite set of values of \mathbf{G} . These order parameters are constrained by the sum rules of Eq. (21) and also by the condition $\sum_n \langle \rho_{n,n}(\mathbf{r}) \rangle = \tilde{\nu}$. In the bilayer case, this condition imposes $\langle \rho_{0,0}(\mathbf{G}) \rangle = -\langle \rho_{1,1}(\mathbf{G}) \rangle$ for $\mathbf{G} \neq 0$. This severe constraint does not allow the crystal state to take full advantage of the non-monotonous behavior of the effective interaction in distributing its weight amongst the order parameters with different \mathbf{G}' s. By contrast, the trilayer's constraint $\langle \rho_{0,0}(\mathbf{G}) \rangle + \langle \rho_{1,1}(\mathbf{G}) \rangle + \langle \rho_{2,2}(\mathbf{G}) \rangle = 0$ is much less severe. This point has been discussed on symmetry grounds in Ref. 12. The effective theory describing the CCP to IUP phase transition requires the presence of third order term which, based on symmetry arguments, vanish for any two-level system such as bilayer graphene.

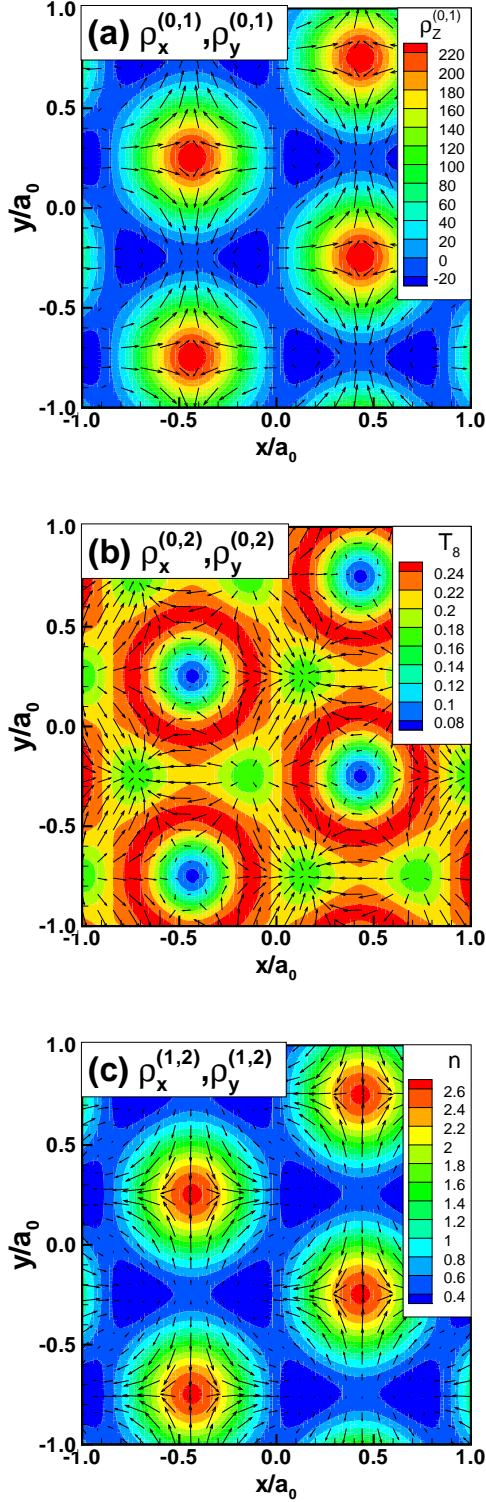


FIG. 7: (Color online) Pseudospin texture in the (a) $(0,1)$; (b) $(0,2)$; (c) $(1,2)$ pseudospin systems for the crystal state at $\nu = 1$, $\Delta_{LL} = 0$ and $B = 10$ T. The total electronic density and $T_8(\mathbf{r})$ are shown in the contour plots of (c) and (d) respectively.

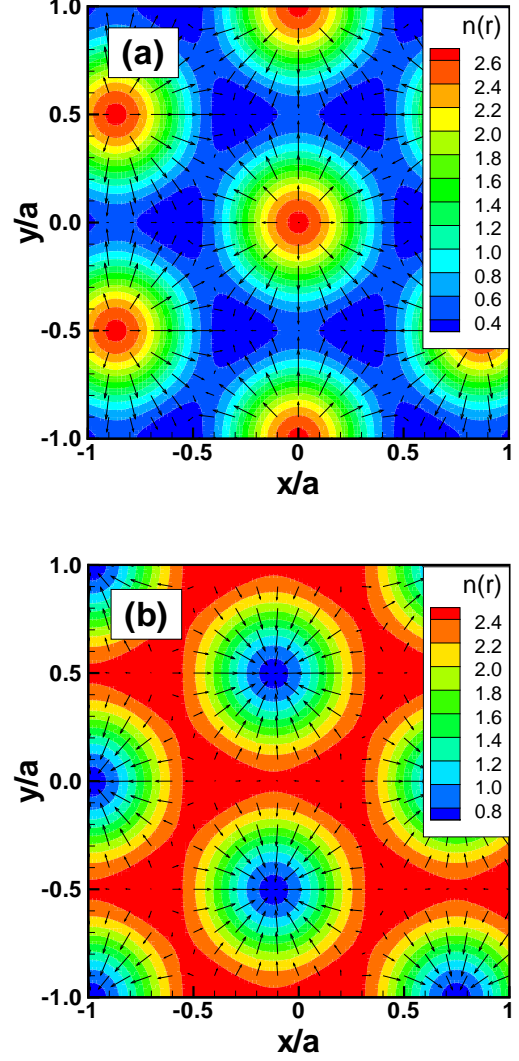


FIG. 8: (Color online) Electronic density and dipole field in the crystal state for (a) $\tilde{\nu} = 1$ and (b) $\tilde{\nu} = 2$. Parameters are $\Delta_{LL} = 0$ and $B = 10$ T.

VIII. PROPERTIES OF THE CRYSTAL STATE

In this section, we look at some of the properties of the coherent crystal state in more details.

A. Density of states

The density of states in the IUP and CP for $\tilde{\nu} = 1$ and $\Delta_{LL} = 0, B = 10$ T is shown in Fig. 11. In the IUP, the three peaks correspond to the energies E_n^0 (see Eq. (10)) of the three levels $n = 0, 1, 2$ renormalized by the exchange interaction. The band structure of the crystal has three peaks, as expected for a crystal with filling factor $\tilde{\nu} = 1$, but slightly displaced in energy and broadened

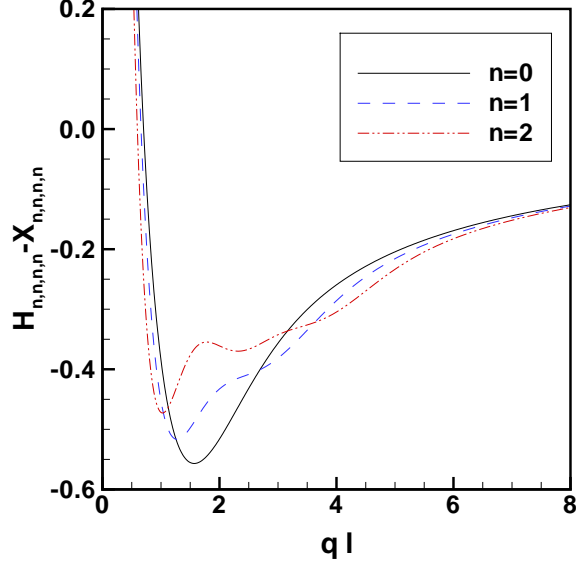


FIG. 9: (Color online) Effective Hartree-Fock interaction in orbitals $n = 0, 1, 2$.

due to the finite bandwidth of each band in the crystal state. The lowest-energy band is fully filled while the other two bands are empty. From this figure, we see that the electron-hole continuum in the crystal state occurs in the energy range $E \in [0.6, 1.2] e^2/\kappa\ell$ approximately.

B. Collective excitations, absorption spectrum and quantum Hall plateaus

The absorption spectrum for the IUP has one peak at the frequency $\omega_{IUP}(\mathbf{q} = 0)$ calculated in Eq. (56) which corresponds to the gap in the first collective mode. The second dispersive mode shows up in the response functions $\chi_{\rho_{x,y}^{(0,2)}, \rho_{x,y}^{(0,2)}}^{(R)}$ and since $\rho_{x,y}^{(0,2)}$ are not part of the dipole definition, it does not lead to electromagnetic absorption.

The collective mode spectrum in the crystal phase is more complex. Fig. 12 shows the dispersion relations for $\tilde{\nu} = 1$, $B = 10$ T and $\Delta_{LL} = 0$. Only the first low-energy modes that are below the electron-hole continuum are shown. The first, gapless, mode is the magnetophonon mode. It has the typical $\omega \sim q^{3/2}$ dispersion associated with the magnetophonon mode of a Wigner crystal³². The other modes are gapped and correspond to more local deformations of the density. All modes are accompanied by fluctuations of the pseudospins.

We can get an idea of the nature of the mode at $\mathbf{q} = 0$ by computing the response functions $\chi_{\rho_{\alpha}^{(i,j)}, \rho_{\alpha}^{(i,j)}}^{(R)}(\mathbf{q} = 0, \mathbf{q} = 0, \omega)$ with $\alpha = x, y$ and $(i, j) = (0, 1), (1, 2), (0, 2)$ from the pseudospins defined in Sec. IV. We find that the first gapped mode appears as a

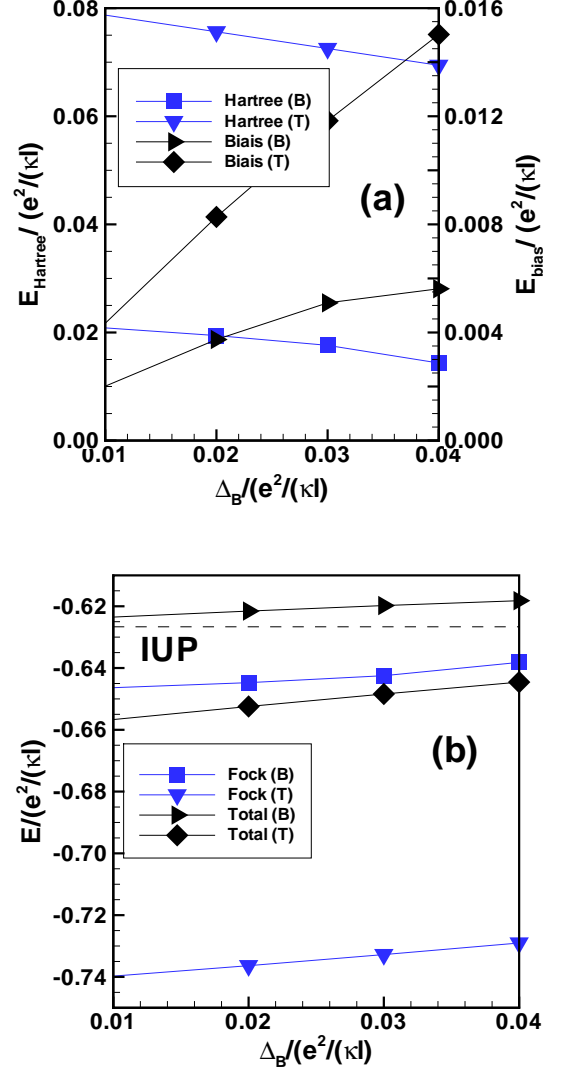


FIG. 10: (Color online) Contribution of different terms to the total energy of the crystal state in bilayer (B) and trilayer (T) graphene for $\tilde{\nu} = 1$ and $B = 10$ T. (a) Hartree and bias energies; (b) Fock and total energies. The dashed line is the total energy of the incoherent uniform phase.

pole of $\chi_{\rho_{x,y}^{(0,1)}, \rho_{x,y}^{(0,1)}}^{(R)}$ and $\chi_{\rho_{x,y}^{(1,2)}, \rho_{x,y}^{(1,2)}}^{(R)}$ but not of $\chi_{\rho_{x,y}^{(0,2)}, \rho_{x,y}^{(0,2)}}^{(R)}$ while it is just the opposite for the second gapped mode. We can thus expect that the first gapped mode will be active in the absorption while the second gapped mode will not. This is confirmed by a direct calculation of the absorption spectrum $P_x(\omega)$ as shown in Fig. 13 for the crystal state at $\Delta_{LL} = 0.09e^2/\kappa\ell$. Fig. 13 also shows the change in the absorption spectrum when Δ_{LL} is increased from $\Delta_{LL} = 0.09e^2/\kappa\ell$, in the crystal phase, to $\Delta_{LL} = 0.1e^2/\kappa\ell$ where the C2DEG has transitioned to the incoherent uniform phase. Such a change should be observable experimentally.

The Coulomb energy $e^2/\kappa\ell = 56.2\sqrt{B}$ meV with B

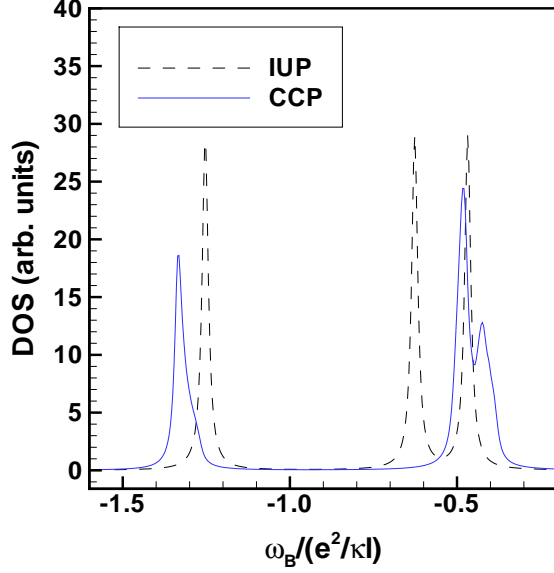


FIG. 11: (Color online) Density of states in the incoherent uniform phase (IUP) and coherent crystal phase (CCP) for $\tilde{\nu} = 1$, $\Delta_{LL} = 0$ and $B = 10$ T.

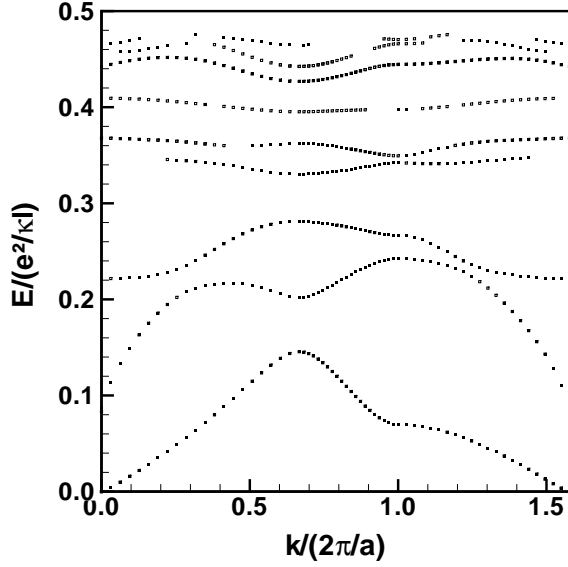


FIG. 12: Dispersion relation of the collective modes of the crystal phase at $\tilde{\nu} = 1$, $\Delta_{LL} = 0$ and $B = 10$ T.

in Tesla and $\kappa = 1$. At $B = 10$ T, this gives $e^2/\kappa\ell = 4.3 \times 10^{13}$ Hz. The frequency of the first gapped mode is at the upper limit of the microwave spectrum. It can be pushed down, however, by increasing the dielectric constant κ of the substrate. Note that the crystal state would likely be pinned by disorder. In this case, the magnetophonon mode would be gapped and there would

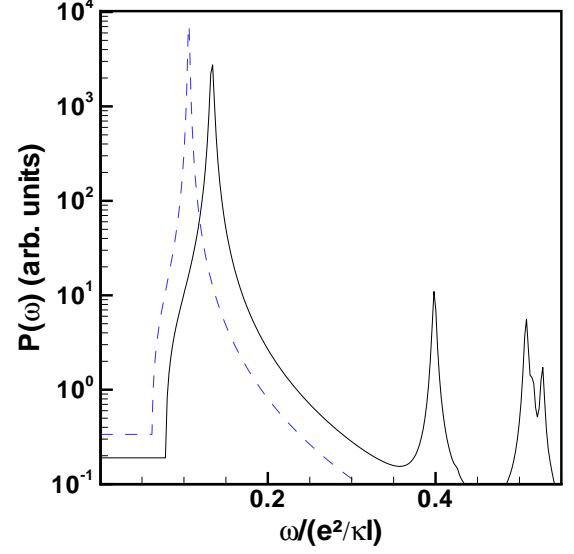


FIG. 13: (Color online) Comparison of the absorption in the incoherent uniform phase at $\Delta_{LL} = 0.1e^2/\kappa\ell$ (dashed blue line) and in the coherent crystal phase (full black line) at $\Delta_{LL} = 0.09e^2/\kappa\ell$. We choose $\tilde{\nu} = 1$ and $B = 10$ T in both cases.

be a corresponding absorption at the pinning frequency corresponding to this gap. The pinning frequency would then depend on the level of disorder in the system.

The transition from the IUP to CP should also show up in the Hall conductivity. As we just said, the crystal state would be pinned by disorder leading to insulating behavior of the electrons in the uppermost Landau level. When $\tilde{\nu} = 1, 2$, this means that the quantized Hall conductivity should have a value corresponding to the *adjacent* interaction driven integer quantum Hall plateau. For example, if the ground state stays crystalline in a small region around filling factor $\nu = -5$ (corresponding to $\tilde{\nu} = 1$), there should be a dip in the Hall plateau from $\sigma_{xy} = -5e^2/h$ to $\sigma_{xy} = -6e^2/h$ in this region.

IX. CONCLUSION

We have studied the phase diagram of the two-dimensional electron gas in an ABC-stacked graphene tri-layer in Landau level $N = 0$. Our analysis is restricted to the integer filling factors such as $\nu = -5, -4$ and $\nu = 4, 5$ where spin and layer pseudospin degrees of freedom can be considered as frozen. We used a three-level system consisting of three Landau orbitals $n = 0, 1, 2$ which are separated by an energy gap Δ_{LL} (this gap is related to an applied potential bias between the outermost layers) and considered Coulomb interaction in the Hartree-Fock approximation.

We calculated the energies of different uniform and

non-uniform phases of the C2DEG as Δ_{LL} is varied from negative to positive values at integer filling factors $\tilde{\nu} = 1, 2$ of the three-level system. Our results show a phase diagram for the ABC-stacked trilayer graphene that is very different from its bilayer cousin. The ground state in the trilayer is an incoherent uniform phase at large value of $|\Delta_{LL}|$ and a coherent crystal phase in between. In the incoherent uniform phase, electrons fully occupy the lowest-energy orbitals. In the coherent crystal phase, there is one electron per unit cell of a triangular crystal lattice and this electron is in a linear combination of the three orbital states. Around each lattice site of the crystal, we find an intricate orbital pseudospin texture with a finite density of electric dipoles in the plane of the layers. The fact that the crystal state also occurs at positive value of Δ_{LL} is specific to trilayer graphene or, more generally, to C2DEG with chirality index $J > 2$.

We studied some transport and optical properties of the two phases involved in the phase diagram. The crystal has a phonon mode that, when disorder is included in the calculation, should be gapped at $\mathbf{q} = 0$. The corresponding pinning mode should then be observable in microwave absorption experiment. The crystal has also higher-energy modes which are active in electromagnetic absorption. By contrast, only one mode should show up in the absorption spectrum of the incoherent uniform phase. It should thus be possible to localize the transition between these two states experimentally.

Another experimental signature of the crystal state is that, if disorder localizes all electrons in the uppermost Landau level, then a measurement of the Hall conductivity should show a quantization at a value corresponding to the *adjacent* interaction driven integer quantum Hall plateau.

Acknowledgments

R. Côté was supported by a grant from the Natural Sciences and Engineering Research Council of Canada (NSERC). Computational resources were provided by Compute Canada and Calcul Québec.

Appendix A: FOCK INTERACTIONS IN THE UNIFORM PHASES

In the uniform phases, we need to evaluate the Hartree and Fock interactions for $\mathbf{q} = 0$. The Hartree interactions are zero and the only nonzero Fock interactions are (in units of $\sqrt{\pi/2}e^2/\kappa\ell$):

$$X_{0,0,0,0}(0) = 1, X_{1,1,1,1}(0) = \frac{3}{4}, \quad (\text{A1})$$

$$X_{2,2,2,2}(0) = \frac{41}{64}, \quad (\text{A2})$$

$$X_{0,0,2,2}(0) = X_{2,2,0,0}(0) = \frac{3}{8}, \quad (\text{A3})$$

$$X_{2,0,0,2}(0) = X_{0,2,2,0}(0) = \frac{3}{8}, \quad (\text{A4})$$

$$X_{2,2,1,1}(0) = X_{1,1,2,2}(0) = \frac{7}{16}, \quad (\text{A5})$$

$$X_{1,2,2,1}(0) = X_{2,1,1,2}(0) = \frac{7}{16}, \quad (\text{A6})$$

$$X_{0,0,1,1}(0) = X_{1,1,0,0}(0) = \frac{1}{2}, \quad (\text{A7})$$

$$X_{1,0,0,1}(0) = X_{0,1,1,0}(0) = \frac{1}{2}, \quad (\text{A8})$$

$$X_{0,1,2,1}(0) = X_{1,0,1,2}(0) = \frac{1}{\sqrt{32}}, \quad (\text{A9})$$

$$X_{1,2,1,0}(0) = X_{2,1,0,1}(0) = \frac{1}{\sqrt{32}}. \quad (\text{A10})$$

Appendix B: HARTREE-FOCK AND GRPA EQUATIONS

The equation of motion for the Green's function in the Matsubara formalism and in the Hartree-Fock approximation is given by

$$\begin{aligned} & (i\omega_n + \mu/\hbar - E_{n_1}^0) G_{n_1, n_2}(\mathbf{q}, i\omega_n) \\ & - \sum_{\mathbf{q}'} \gamma_{\mathbf{q}, \mathbf{q}'} U_{n_1, n_3}^{(H)}(\mathbf{q} - \mathbf{q}') G_{n_3, n_2}(\mathbf{q}, i\omega_n) \\ & + \sum_{\mathbf{q}'} \gamma_{\mathbf{q}, \mathbf{q}'} U_{n_1, n_3}^{(F)}(\mathbf{q} - \mathbf{q}') G_{n_3, n_2}(\mathbf{q}, i\omega_n) \\ & = \delta_{n_1, n_2} \delta_{\mathbf{q}, 0}, \end{aligned} \quad (\text{B1})$$

where

$$\gamma_{\mathbf{q}, \mathbf{q}'} = e^{-i\mathbf{q} \times \mathbf{q}' \ell^2 / 2} \quad (\text{B2})$$

and

$$U_{n_3, n_4}^H(\mathbf{q}) = H_{n_1, n_2, n_3, n_4}(-\mathbf{q}) \langle \rho_{n_1, n_2}(\mathbf{q}) \rangle, \quad (\text{B3})$$

$$U_{n_3, n_4}^F(\mathbf{q}) = X_{n_1, n_4, n_3, n_2}(-\mathbf{q}) \langle \rho_{n_1, n_2}(\mathbf{q}) \rangle. \quad (\text{B4})$$

The self-consistent Eq. (B1) can be put in a matrix form by defining super-indices. It must then be solved numerically in an iterative way in order to get the order parameters in the different orbital phases.

In the GRPA, $\chi_{n_1, n_2, n_3, n_4}(\mathbf{q}, \mathbf{q}'; \tau)$ is the solution of the equation

$$\begin{aligned}
& \chi_{n_1, n_2, n_3, n_4}(\mathbf{q}, \mathbf{q}'; i\Omega_n) \\
= & \chi_{n_1, n_2, n_3, n_4}^{(0)}(\mathbf{q}, \mathbf{q}'; i\Omega_n) \\
& + \frac{1}{\hbar} \sum_{\mathbf{q}''} \chi_{n_1, n_2, n_5, n_6}^{(0)}(\mathbf{q}, \mathbf{q}''; i\Omega_n) \\
& \times H_{n_5, n_6, n_7, n_8}(\mathbf{q}'') \chi_{n_7, n_8, n_3, n_4}(\mathbf{q}'', \mathbf{q}'; i\Omega_n) \\
& - \frac{1}{\hbar} \sum_{\mathbf{q}''} \chi_{n_1, n_2, n_5, n_6}^{(0)}(\mathbf{q}, \mathbf{q}''; i\Omega_n) \\
& \times X_{n_5, n_8, n_7, n_6}(\mathbf{q}'') \chi_{n_7, n_8, n_3, n_4}(\mathbf{q}'', \mathbf{q}'; i\Omega_n),
\end{aligned} \tag{B5}$$

where Ω_n is a bosonic Matsubara frequency and the Hartree-Fock two-particle Green's function $\chi_{n_1, n_2, n_3, n_4}^{(0)}(\mathbf{q}, \mathbf{q}'; i\Omega_n)$ is given by

$$\begin{aligned}
& [i\hbar\Omega_n - (E_{n_2}^0 - E_{n_1}^0)] \chi_{n_1, n_2, n_3, n_4}^{(0)}(\mathbf{q}, \mathbf{q}', \Omega_n) \\
= & \hbar\gamma_{\mathbf{q}, \mathbf{q}'}^* \langle \rho_{n_1, n_4}(\mathbf{q} - \mathbf{q}') \rangle \delta_{n_2, n_3} \\
& - \hbar\gamma_{\mathbf{q}, \mathbf{q}'} \langle \rho_{n_3, n_2}(\mathbf{q} - \mathbf{q}') \rangle \delta_{n_1, n_4} \\
& - \sum_{\mathbf{q}''} \gamma_{\mathbf{q}, \mathbf{q}''}^* U_{m, n_1}^{(H)}(\mathbf{q} - \mathbf{q}'') \chi_{m, n_2, n_3, n_4}^{(0)}(\mathbf{q}'', \mathbf{q}', \Omega_n) \\
& + \sum_{\mathbf{q}''} \gamma_{\mathbf{q}, \mathbf{q}''} U_{n_2, m}^{(H)}(\mathbf{q} - \mathbf{q}'') \chi_{n_1, m, n_3, n_4}^{(0)}(\mathbf{q}'', \mathbf{q}', \Omega_n) \\
& + \sum_{\mathbf{q}''} \gamma_{\mathbf{q}, \mathbf{q}''}^* U_{m, n_1}^{(F)}(\mathbf{q} - \mathbf{q}'') \chi_{m, n_2, n_3, n_4}^{(0)}(\mathbf{q}'', \mathbf{q}', \Omega_n) \\
& - \sum_{\mathbf{q}''} \gamma_{\mathbf{q}, \mathbf{q}''} U_{n_2, m}^{(F)}(\mathbf{q} - \mathbf{q}'') \chi_{n_1, m, n_3, n_4}^{(0)}(\mathbf{q}'', \mathbf{q}', \Omega_n).
\end{aligned} \tag{B6}$$

Note that the response functions depend only on the order parameters $\langle \rho_{n, m}(\mathbf{q}) \rangle$ computed in the HFA. Eqs. (B5, B6) can be solved numerically by writing them in a matrix form defining super-indices.

Appendix C: INFINITESIMAL GENERATORS OF SU(3)

Our system has a SU(3) representation. The infinitesimal generators of this representation are given by the traceless Hermitian matrices

$$T_a = \frac{\lambda_a}{2}, \tag{C1}$$

where, in the basis (0, 1, 2):

$$\lambda_1 = \begin{pmatrix} 0 & 1 & 0 \\ 1 & 0 & 0 \\ 0 & 0 & 0 \end{pmatrix}, \lambda_2 = \begin{pmatrix} 0 & -i & 0 \\ i & 0 & 0 \\ 0 & 0 & 0 \end{pmatrix}, \tag{C2}$$

$$\lambda_3 = \begin{pmatrix} 1 & 0 & 0 \\ 0 & -1 & 0 \\ 0 & 0 & 0 \end{pmatrix}, \lambda_4 = \begin{pmatrix} 0 & 0 & 1 \\ 0 & 0 & 0 \\ 1 & 0 & 0 \end{pmatrix}, \tag{C3}$$

$$\lambda_5 = \begin{pmatrix} 0 & 0 & -i \\ 0 & 0 & 0 \\ i & 0 & 0 \end{pmatrix}, \lambda_6 = \begin{pmatrix} 0 & 0 & 0 \\ 0 & 0 & 1 \\ 0 & 1 & 0 \end{pmatrix}, \tag{C4}$$

and

$$\lambda_7 = \begin{pmatrix} 0 & 0 & 0 \\ 0 & 0 & -i \\ 0 & i & 0 \end{pmatrix}, \lambda_8 = \frac{1}{\sqrt{3}} \begin{pmatrix} 1 & 0 & 0 \\ 0 & 1 & 0 \\ 0 & 0 & -2 \end{pmatrix}. \tag{C5}$$

With these generators, we can define eight real fields $\tilde{F}_a(\mathbf{r}) = \Phi^\dagger(\mathbf{r}) T_a \Phi(\mathbf{r})$ with the Fourier transform

$$\tilde{F}_a(\mathbf{q}) = \int d\mathbf{r} e^{-i\mathbf{q}\cdot\mathbf{r}} \Phi^\dagger(\mathbf{r}) T_a \Phi(\mathbf{r}). \tag{C6}$$

These fields are related to the pseudospin fields by the relations:

$$F_1(\mathbf{q}) = \beta_q \rho_x^{(0,1)}(\mathbf{q}), F_2(\mathbf{q}) = \beta_q \rho_y^{(0,1)}(\mathbf{q}), \tag{C7}$$

$$F_3(\mathbf{q}) = \beta_q \rho_z^{(0,1)}(\mathbf{q}), \tag{C8}$$

$$F_4(\mathbf{q}) = \beta_q \rho_x^{(0,2)}(\mathbf{q}), F_5(\mathbf{q}) = \beta_q \rho_y^{(0,2)}(\mathbf{q}), \tag{C9}$$

$$F_6(\mathbf{q}) = \beta_q \rho_x^{(1,2)}(\mathbf{q}), F_7(\mathbf{q}) = \beta_q \rho_y^{(1,2)}(\mathbf{q}), \tag{C10}$$

and

$$F_8(\mathbf{q}) = \frac{1}{2\sqrt{3}} \beta_q (\rho_{0,0}(\mathbf{q}) + \rho_{1,1}(\mathbf{q}) - 2\rho_{2,2}(\mathbf{q})), \tag{C11}$$

where we have defined

$$\rho_x^{(i,j)} = \frac{1}{2} (\rho_{i,j} + \rho_{j,i}), \tag{C12}$$

$$\rho_y^{(i,j)} = \frac{1}{2i} (\rho_{i,j} - \rho_{j,i}), \tag{C13}$$

$$\rho_z^{(i,j)} = \frac{1}{2} (\rho_{i,i} - \rho_{j,j}). \tag{C14}$$

¹ K. S. Novoselov, A. K. Geim, S. V. Morozov, D. Jiang, M. I. Katsnelson, I. V. Grigorieva, S. V. Dubonos, A. A.

Firsov, Nature **438**, 197 (2005).
² Y. B. Zhang, Yan-Wen Tan, Horst L. Stormer, Philip Kim,

- Nature **438**, 201 (2005).
- ³ Edward McCann and Vladimir I. Fal'ko, Phys. Rev. Lett. **96**, 086805 (2006).
 - ⁴ K. S. Novoselov, E. McCann, S. V. Morozov, V. I. Fal'ko, M. I. Katsnelson, U. Zeitler, D. Jiang, F. Schedin and A. K. Geim, Nature Physics **2**, 177 (2006).
 - ⁵ Liyuan Zhang, Yan Zhang, Jorge Camacho, Maxim Khodas and Igor Zaliznyak, Nature Physics **7**, 953 (2011); W. Bao, L. Jing, J. Velasco Jr, Y. Lee, G. Liu, D. Tran, B. Standley, M. Aykol, S. B. Cronin, D. Smirnov, M. Koshino, E. McCann, M. Bockrath and C. N. Lau, Nature Physics **7**, 948 (2011); A. Kumar, W. Escoffier, J. M. Poumiro, C. Faugeras, D. P. Arovas, M. M. Fogler, F. Guinea, S. Roche, M. Goiran, and B. Raquet, Phys. Rev. Lett. **107**, 126806, 2011; S. Yuan, R. Roldan and M. I. Katsnelson, Phys. Rev. B **84**, 125455 (2011); E. A. Henriksen, D. Nandi, and J. P. Eisenstein, Phys. Rev. X **2**, 011004 (2012).
 - ⁶ Hongki Min and A. H. MacDonald, Phys. Rev. B **77**, 155416 (2008).
 - ⁷ F. Guinea, A. H. Castro-Neto and N. M. Peres, Phys. Rev. B **73**, 245426 (2006).
 - ⁸ Yafis Barlas, Kun Yang and A. H. MacDonald, Nanotechnology **23**, 052001 (2012).
 - ⁹ K. Nomura and A. H. MacDonald, Phys. Rev. Lett. **96**, 256602, (2006).
 - ¹⁰ Yafis Barlas, R. Côté, K. Nomura, and A. H. MacDonald, Phys. Rev. Lett. **101**, 097601 (2008).
 - ¹¹ Fan Zhang, Dagim Tilahun, and A. H. MacDonald, Phys. Rev. B **85**, 165139, (2012).
 - ¹² Yafis Barlas, R. Côté, and Maxime Rondeau, unpublished. arXiv:1112.2729v1.
 - ¹³ Benjamin E. Feldman, Jens Martin and Amir Yacoby, Nat. Phys. **5**, 889 (2009); Y. Zhao, P. Cadden-Zimansky, Z. Jiang, and P. Kim, Phys. Rev. Lett. **104**, 066801 (2010).
 - ¹⁴ Thiti Taychatanapat, Kenji Watanabe, Takashi Taniguchi and Pablo Jarillo-Herrero, Nature Phys. **7**, 621 (2011).
 - ¹⁵ Yafis Barlas, R. Côté, J. Lambert, and A. H. MacDonald, Phys. Rev. Lett. **104**, 096802 (2010).
 - ¹⁶ R. Côté, Jules Lambert, Yafis Barlas, and A. H. MacDonald, Phys. Rev. B **82**, 035445 (2010).
 - ¹⁷ R. Côté, J. P. Fouquet, and Wenchen Luo, Phys. Rev. B **84**, 235301 (2011).
 - ¹⁸ X. Z. Yu, Y. Onose, N. Kanazawa, J. H. Park, J. H. Han, Y. Matsui, N. Nagaosa and Y. Tokura, Nature **465**, 901 (2010).
 - ¹⁹ Jung Hoon Han, Jiadong Zang, Zhihua Yang, Jin-Hong Park, and Naoto Nagaosa, Phys. Rev. B **82**, 094429 (2010).
 - ²⁰ Jin-Hong Park and Jung Hoon Han, Rev. Rev. B **83**, 184406 (2011).
 - ²¹ I. Dzyaloshinsky, J. Phys. Chem. Solids **4**, 241 (1958); T. Moriya, Phys. Rev. **120**, 91 (1960).
 - ²² Mikito Koshino and Edward McCann, Phys. Rev. B **80**, 165409 (2009).
 - ²³ Fan Zhang, Bagawan Sahu, Hongki Min, and A. H. MacDonald, Phys. Rev. B **82**, 035409 (2010).
 - ²⁴ We remark that because of our particular definition of the ladder operators, we have $a^\dagger h_{n,X}(\mathbf{r}) = i\sqrt{n+1}h_{n+1,X}(\mathbf{r})$ and $ah_{n,X}(\mathbf{r}) = -i\sqrt{n}h_{n-1,X}(\mathbf{r})$.
 - ²⁵ R. Côté, Manuel Barrette, Maxime Rondeau and Yafis Barlas, unpublished.
 - ²⁶ See for example: David Pines and Philippe Nozières, *The theory of quantum liquids* vol. 1, W. A. Benjamin, New York, (1966).
 - ²⁷ J. P. Elliott and P. G. Dawabber, Symmetry in physics, vol. 1, MacMillan, London, (1979).
 - ²⁸ K. Shizuya, Phys. Rev. B **79**, 165402 (2009).
 - ²⁹ For $\mathbf{q} \neq 0$, the total current also contains a contribution that can be written as the curl of a magnetization density.
 - ³⁰ Sankalpa Gosh and R. Rajamaran, Phys. Rev. B **63**, 035304 (2000).
 - ³¹ Zyun F. Ezawa, *Quantum Hall effects*, World Scientific, London (2008).
 - ³² L. Bonsall and A. A. Maradudin, Phys. Rev. B **15**, 1959 (1977).